Microsized Graphene Helmholtz Resonator on Circular Dielectric Rod: A Tunable Sub-THz Frequency-Selective Scatterer

Alexander Ye. Svezhentsev, *Senior Member, IEEE*, Sergii V. Dukhopelnykov, *Member, IEEE*, Vladimir Volski, *Member, IEEE*, Guy A. E. Vandenbosch, *Fellow, IEEE*, and Alexander I. Nosich, *Fellow, IEEE*

***Abstract*—A novel miniature THz resonator consisting of a finite-length slotted graphene cylinder wrapped around an infinite circular dielectric rod is proposed. A full-wave 3-D electromagnetic scattering model is built using the method of moments (MoM) solution of the electric-field integral equation (EFIE) in the spectral domain. In order to gain a better understanding of the associated physical effects, the obtained results are compared with a 2-D model where the slotted graphene cylinder is assumed infinite. A good agreement between the 3-D and 2-D models is found. The dependence of the backscattering radar cross section on the frequency is analyzed. It is found that in both cases this scatterer displays quasi-static Helmholtz resonance (HR) response in the sub-THz frequency range, a behavior previously known for perfectly electrically conducting (PEC) slotted cylinders. For both models, in-resonance surface current distributions and far-zone radiation patterns are given. The most important innovation is that due to the use of graphene the Helmholtz-mode resonance becomes electrically tunable.**

***Index Terms*—Conformal antennas, graphene patch, Helmholtz resonance (HR), hyper-singular integral equation, method of moments (MoM), radar cross section.**

I. Introduction

THE Helmholtz resonance (HR) has been known since at least the middle ages as a remarkable acoustic phenomenon observed on rigid cavities with narrow throats. In the 19th century, it was demystified by Helmholtz who published an approximate but efficient description of this effect [1]. Rayleigh [2] gave the mathematical theory of canonical-shape HR–rigid sphere with a circular hole. This theory was refined in [3]. Perhaps, the most well-known application today of HR concerns the design of submerged sonar targets and absorbers for car mufflers.

More than a hundred years later, an electromagnetic analog of the HR effect was found in the microwave range in the form of the so-called slot wave propagating on a hollow metal waveguide with a longitudinal slot [4].

A full-wave theory of this effect was built for a 2-D zero-thickness slotted circular perfectly electrically conducting (PEC) cylinder in the free space [5], and on a circular dielectric rod [6]–[9]. In the latter case, elementary dipole excitation was studied in [10]. Later the HR effect on the slot mode was studied in [11] in the 2-D scattering and absorption by a resistive slotted cylinder in the free space.

Note that an electromagnetic analog of the acoustic-mode HR does not exist on a PEC sphere with a circular hole [12]. However, if a PEC or well-conducting cavity resembles a finite section of a slotted hollow waveguide, then a similar mode may exist in the transverse-electric polarization, as described for the slotted box gold cavity in the infrared range [13]. Note also that the HR effect was verified experimentally in [14].

It should be mentioned that 2-D scattering problems connected with cylinders are of interest in the literature [15]–[19]. In particular, in [15] a cylindrical strip is arranged on a dielectric cylinder surface, in [16] a metal cylinder placed in a flat dielectric layer is excited by a current-carrying skew strip. The authors of [17] studied multiple scattering by random configurations of circular cylinders. In [18] and [19], the scattering problem is solved for anisotropic cylinders. Interesting ideas concerning the method of moments (MoM) solution of scattering from PEC scatterers composed of mixtures of smooth and non-smooth geometrical features can be found in [20].

Among the mentioned papers [15]–[20], [15] is the closest to the subject of our research. However, in that work, the E-polarization case is considered and therefore there is no HR, which is the core phenomenon in this article.

A distinctive feature of the Helmholtz mode in acoustics is its quasi-static nature [1]–[3]. In electromagnetics, this corresponds to the LC-contour description, see [5], [6]. As a result, in the 2-D PEC model, the HR frequency tends to zero for an angular width of the slot going to zero [5]–[9]. In the

Manuscript received December 18, 2020; revised July 7, 2021; accepted September 6, 2021. Date of publication October 14, 2021; date of current version March 3, 2022. The work of Sergii V. Dukhopelnykov was supported in part by the National Research Foundation of Ukraine under Grant 2020-02-0150. *(Corresponding author: Alexander Ye. Svezhentsev.)*

Alexander Ye. Svezhentsev, Sergii V. Dukhopelnykov, and Alexander I. Nosich are with O. Y. Usikov Institute of Radiophysics and Electronics, National Academy of Sciences of Ukraine, 61085 Kharkiv, Ukraine (e-mail: oleksandr.svezhentsev@gmail.com).

Vladimir Volski and Guy A. E. Vandenbosch are with the Division of ESAT-WaveCoRE, Katholieke Universiteit Leuven, 3001 Leuven, Belgium (e-mail: guy.vandenbosch@kuleuven.be).

Color versions of one or more figures in this article are available at https://doi.org/10.1109/TAP.2021.3118840.

Digital Object Identifier 10.1109/TAP.2021.3118840

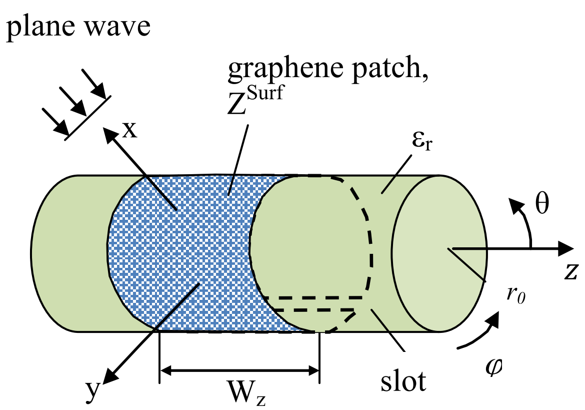

Fig. 1. Plane wave excitation of finite slotted graphene cylinder placed on the surface of infinite circular dielectric rod.

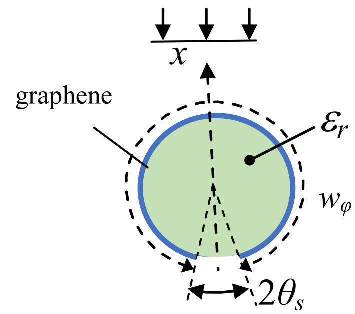

Fig. 2. Cross-sectional view of the scattering of an H-polarized plane wave from a graphene slotted cylinder on a circular dielectric rod.

3-D case, this should not be the same although the natural frequency can be very small; one can expect that the minimum value depends on the length of the cavity.

As for graphene cavities, the 2-D scattering from a dielectric rod with a conformal slotted cover was recently studied in [21] and [22]. This analysis revealed the Helmholtz-mode resonance in the THz or infrared range, depending on the rod radius. It is crucial to realize that here HR becomes electrically tunable because its frequency depends on the graphene surface impedance.

In this work, we study the 3-D configuration shown in Fig. 1. On the surface of an infinitely long circular dielectric rod along the z-axis, a patch made of graphene is located. The patch is shaped as a finite slotted graphene cylinder with an arbitrary angular slot width. The mathematical model of the plane-wave scattering from such a scatterer is built using the electric-field integral equation (EFIE) for the surface current on the patch and an MoM-Galerkin scheme in the spectral domain using piecewise sinusoidal (PWS) basis functions. This solution is similar to the one built earlier for PEC conformal array antennas [23]–[25] and for periodical arrays [26]. In particular, in [26] the low-frequency HR was analyzed for an array of PEC patches placed in an azimuthally periodic manner on the surface of the infinite dielectric rod.

As a reference, we use the 2-D model, in which not only the dielectric rod but also the slotted graphene cylinder is infinite, analyzed using the approach of [21], [22]. This approach also uses the EFIE, which is a hyper-singular equation, discretized with the aid of the guaranteed-convergence Nystrom quadrature interpolation scheme.

The novelty in this article consists of the following points. First, the MoM solution for PEC patches periodically placed on a dielectric rod surface [26] is extended to structures with resistive patches described via a surface impedance. As a consequence, a new term in the resulting impedance coupling matrix appears, which is obtained in an explicit form. Second, for the first time graphene is used as the material for the finite slotted cylinder. Third, we show that the 3-D graphene resonators are able to support a Helmholtz-like mode, a phenomenon not studied in the literature before. Besides, in addition to the H-polar case, some results for the E-polar case are presented for the first time.

We make such a study for a resonator explained above and quantify the HR frequency, surface current, and backward scattering cross section (BSCS). Our results are supported by good agreement with the results obtained for the 2-D model, provided that the length of finite graphene slotted exceeds the rod radius more than three times.

Partial preliminary results of our study were presented in the conference paper [27]. However, here they are considerably deepened and extended, together with an in-detail discussion of the slot-mode characteristics. Besides, the tunability of the analyzed resonator with the aid of the chemical potential of graphene is demonstrated and discussed. Note that in [28] the practical realization of a tunable graphene mid-IR biosensor is based on a planar array made of graphene strips. Additionally, although graphene micro and nanotubes are still somewhat exotic objects, they are already being fabricated and studied—see, for instance [29].

II. Infinite Slotted Graphene Cylinder

As a reference, we will use the results obtained for the H-polarized plane wave scattering from the infinite in z-direction circular dielectric rod, covered with an infinite graphene slotted cylinder, see Fig. 2. The scattering problem formulation for the H_z field component is a standard one and involves the Helmholtz equation at $r \neq r_0$, the dielectric-interface boundary conditions at $r = r_0$ off the graphene arc, and the resistive-type boundary condition on that arc. The latter condition has the following form:

$$\vec{E}_{\tan}^{tot,1} + \vec{E}_{\tan}^{tot,2} = 2Z_{surf}\vec{n} \times \left(\vec{H}_{\tan}^{tot,1} - \vec{H}_{\tan}^{tot,2}\right), \quad \vec{E}_{\tan}^{tot,1} = \vec{E}_{\tan}^{tot,2} \tag{1}$$

where Z_{surf} is the surface impedance of graphene (also called *resistivity*) and $\vec{n}$ is the outer unit normal vector. Note that if $Z_{surf} = 0$, then (1) turns to the PEC boundary condition. To provide the solution uniqueness, the edge condition, defining the field behavior near the graphene sharp edges, and the Sommerfeld radiation condition at infinity are used.

The graphene surface impedance is inverse to the surface conductivity σ

$$Z_{surf} = 1/\sigma \tag{2}$$

and the latter quantity is expressed as a Kubo sum [30]

$$\sigma = \sigma_{\text{intra}} + \sigma_{\text{inter}} \tag{3}$$

where

$$\sigma_{\text{intra}} = \frac{c_1}{i\omega + \tau^{-1}}, \quad \sigma_{\text{inter}} = \frac{-iq_e^2}{4\pi h} \ln \frac{2|\mu_c| - (\omega - i\tau^{-1})h}{2|\mu_c| + (\omega - i\tau^{-1})h} \tag{4}$$

$$c_1 = \frac{q_e^2 k_B T}{\pi \hbar^2}\left[\frac{\mu_c}{k_B T} + 2\ln\left(1 + \exp\left(-\frac{\mu_c}{k_B T}\right)\right)\right] \tag{5}$$

ω is the angular frequency, τ is the electron relaxation time, q_e is the electron charge, h is the reduced Planck constant, μ_c is the chemical potential, and T is the temperature. As known, the first term, which is also called the Drude-like term, heavily dominates over the second term at all frequencies below the visible-light range.

The solution to this 2-D problem can be built in several equivalent ways. For instance, we could consider a limit form of the 2-D EFIE in the 3-D problem (this is (10)), obtained after passing to the limit of $w_z \to \infty$ (see Fig. 1), and apply the inverse Fourier transform (IFT) in z-coordinate. The result would be a 1-D hypersingular EFIE for the surface current ϕ-component that can be either analytically regularized as in [11] or solved with a Nystrom algorithm as in [21]. In either case, the convergence of the numerical solution of that EFIE is guaranteed by the mathematical theorems. The solution accuracy is then controlled by the order of discretization. In our analysis, we derive the mentioned hypersingular EFIE via another approach, following [21], [22], and further solve it with a Nystrom algorithm, also presented in [21].

Still, turning back to [11], where the mentioned EFIE for the 2-D scattering problem was reduced to a Fredholm second-kind matrix equation, provides an important analytical result. This is expression (42) for the resonance frequency of the H_{00} mode of a slotted circular cylinder, modified for imperfect conductivity under the assumption that $|Z_{surf}| < Z_0$ (Z_0 being the free-space impedance). Taking into account that in our case graphene is placed on the dielectric rod surface, we obtain

$$f_{res} = \frac{c}{2\pi\ r_0}\left[\left(\frac{-\ln^{-1}\sin(\theta_s/2)}{\varepsilon_r + 1}\right)^{1/2} - \frac{iZ_{surf}}{2Z_0}\right] \times \left[1 + O\left(\frac{|Z_{surf}|}{Z_0}, \frac{1}{\ln\theta_s}\right)\right]. \tag{6}$$

Note that, as the graphene impedance (2) is frequency-dependent, this is not an explicit expression but an equation for f_{res}. It can be cast to a quadratic equation, with the approximate solution given by

$$f_{res} = \frac{c}{2\pi\ r_0}\left(-\frac{1}{\varepsilon_r + 1}\ \ln^{-1}\sin\frac{\theta_s}{2}\right)^{1/2}\left(1 - \frac{c}{2r_0 Z_0 c_1}\right). \tag{7}$$

This equation is accurate within 5% if the slot width is small enough, $2\theta_s \leq 5^o$.

III. Finite Slotted Graphene Cylinder

The final goal in this article is the analysis of a finite slotted graphene cylinder (3-D model) wrapped around an infinite circular dielectric rod with radius r_0 and permittivity ε_r. The angular slot width is $2\theta_s$. The graphene cylinder is finite in the z-direction having the size w_z—see Fig. 1.

This scatterer is excited by a plane wave, which is incident along the direction $-x$, i.e., normally to the rod axis, so that (the time dependence $e^{i\omega t}$ is omitted)

$$\mathbf{E}^{inc} = \mathbf{E}^0 \exp(i\ k_0\ x) \tag{8}$$

where $\mathbf{E}^0$ has the unit amplitude, $k_0 = 2\pi f/c$. Let the angle between the $\mathbf{E}^{inc}$ vector and the z-axis be γ (see [19], [20]), then $\gamma = 0$ and $\gamma = 90$ correspond to the E- and H-polarized plane wave cases, respectively. If γ lies in between these limiting values, then the incident wave contains both polarizations.

The field, scattered from such a composite scatterer, must satisfy: 1) the Maxwell equations off the rod's surface; 2) the dielectric-interface boundary conditions of that surface but off the graphene patch; and 3) the resistive-type boundary condition (2) on that patch. To provide the solution uniqueness, the boundary conditions must be supplemented with the edge conditions on the patch sharp edges and corners, and the radiation condition at infinity.

Here, the radiation condition needs special attention, because we assume that the dielectric rod is infinite. This means that the considered configuration is an open waveguide loaded with an open resonator. Note that the guided waves of such a waveguide do not decay along the rod, i.e., along the z-axis. Therefore, the radiation condition must be adapted to this situation as done in [31], see (36) there.

Similar to [23]–[26], the problem is reduced to EFIE, which follows from the scattered field representation as a convolution of an unknown equivalent surface electric current with the known dielectric-rod Green's function (GF) and the resistive boundary condition (1) on the graphene patch surface $S = \{z, \phi : |z| < w_z/2, \theta_s < \phi < 2\pi - \theta_s\}$

$$\mathbf{E}_s^R(r_0, z, \phi) - \mathbf{E}_s^J(r_0, z, \phi) = \mathbf{E}_s^{0,exc}(r_0, z, \phi) \tag{9}$$

where $\mathbf{E}_s^{0,exc}(r_0, z, \phi)$ is the excitation field, derived from the plane H-polarized wave diffraction from the bare dielectric rod [26], $\mathbf{E}_s^J(r_0, z, \phi)$ is the field created by the surface electric current $\mathbf{J}_s(r_0, \phi', z')$ [23], [26]

$$\mathbf{E}_s^J(r_0, \phi, z) = \iint_{S'} \overline{\mathbf{G}}^J(r_0, r_0, z, z', \phi\ , \phi')\mathbf{J}_s(r_0, \phi', z')\ dS' \tag{10}$$

where $\overline{\mathbf{G}}^J$ is the 3-D dyadic GF of the infinite circular dielectric rod (see Appendix A), and $\mathbf{E}_s^R(r_0, z, \phi)$ is the resistive term expressed as

$$\mathbf{E}_s^R(r_0, z, \phi) = \ Z_{surf}\mathbf{J}_s(r_0, z, \phi). \tag{11}$$

Furthermore, we discretize EFIE (9) using the MoM-Galerkin algorithm developed earlier in the analysis of PEC patch antennas on a circular dielectric rod [26], to obtain

$$\mathbf{Z}\boldsymbol{\alpha} = \mathbf{V} \tag{12}$$

where

$$Z = Z^{NUM} + Z^{AS} + Z^{SURF} + Z^{R} \tag{13}$$

$$Z^{NUM} = \frac{1}{4\pi^2}\sum_{n=-\infty}^{\infty}\int_{h=-\infty}^{\infty}\tilde{\mathbf{J}}^t(r_0,-n,-h) \cdot\left[\tilde{\mathbf{G}}(r_0,n,h)-\tilde{\mathbf{G}}^{AS}(r_0,n,h)-F^S_{n,h}\right]\tilde{\mathbf{J}}^b(r_0,n,h)\,dh \tag{14}$$

$$Z^{AS} = \sum_{n=-\infty}^{\infty}\int_{h=-\infty}^{\infty}\tilde{\mathbf{J}}^t(r_0,-n,-h) \cdot\tilde{\mathbf{G}}^{AS}(n,h)\,\tilde{\mathbf{J}}^b(r_0,n,h)\,dh. \tag{15}$$

$F^S_{n,h}$ and Z^{SURF} stand for the surface wave contribution, Z^{AS} means the contribution of the asymptotes of the spectral GF, Z^R represents a resistive term. Thus, the applied technique incorporates a convergence enhancement in the IFT achieved by subtraction of the asymptotes of the spectral GF in the spectral domain $\tilde{\mathbf{G}}^{AS}(r_0,n,h)$ and by adding its spatial equivalent Z^{AS} in the spatial domain. Besides, the surface wave poles of the spectral GF are compensated by special annihilating functions $F^S_{n,h}$ and the IFT Z^{SURF} is added in the spatial domain in closed form. The formulas (13)–(15) are similar to the ones in [23]–[25], except that now we deal with the GF of the circular DR without an internal metal rod. The spectral GF asymptotes for $n\to\infty$, $h\to\infty$ are obtained by applying asymptotic formulas for modified Bessel and Hankel functions and their derivatives [32, formulas (9.7.7)–(9.7.11)] to the rigorous spectral GF (see Appendix A). Note that the main terms of the GF asymptotes remain the same as in [23]–[25]. Also, the terms $F^S_{n,h}$ and Z^{SURF} are introduced similarly as in [23]–[26].

An essentially new aspect which appears here, in comparison with [23]–[26], consists of the fact that in (12) and (13) a new additional term is introduced, namely the matrix Z^R, and expressed as

$$Z^R = \begin{bmatrix} Z^{R,z,z} & 0 \\ 0 & Z^{R,\varphi,\varphi}\end{bmatrix}. \tag{16}$$

The elements of $Z^{R,z,z}$ and $Z^{R,\varphi,\varphi}$ are calculated in an analytical form (see Appendix B).

As known, the far-zone field, scattered from the configuration shown in Fig. 1, is built of two parts: the spherical wave and the sum of guided waves, supported by the rod.

Our research is focused on the computation of BSCS, also known as monostatic radar cross section. This quantity has the meaning of the power, reflected in the direction, opposite to the propagation direction of the incident plane wave. Therefore, it is related to the spherical-wave part of the scattered field, $\mathbf{E}^{scat,J}(R,\theta,\phi)$ [33], as

$$BSCS_{uv} = 4\pi\lim_{R\to\infty}R^2\left|\mathbf{E}^{scat,J}(R,\theta=\pi/2,\phi=0)\cdot\mathbf{v}\right|^2 \tag{17}$$

where $\mathbf{E}^{scat,J}\cdot\mathbf{v}$ is the spherical wave v-component ($\nu=\theta,\phi$).

IV. Validation of 3-D Model by 2-D Model for H-Polar Case

Our numerical algorithm is built on (12)–(15). In the computations, we take the following structural parameters: $\varepsilon_r = 2.4$, $r_0 = 50\ \mu$m, $\theta_s = 10°$, $w_z = 160\ \mu$m, $W\varphi = 296.67\ \mu$m. As the HR frequency scales with the inverse radius of the rod (7), the chosen radius places this frequency in the sub-THz range, where the graphene impedance is moderate.

The graphene parameters are $\mu_c = 0.5$ eV, $T = 300$ K, and $\tau = 10^{-12}$ s. The latter quantity is deliberately exaggerated to reduce the losses (today, the best samples of graphene have $\tau = 0.5\times10^{-12}$ s).

First, we study the convergence of the algorithm. It is demonstrated in Fig. 3 where $BSCS_{\varphi\varphi}$ (normalized by $2\pi^2 r_0 w_z$) is plotted versus frequency for different values of the segmentation numbers in z and phi-directions, N_Z and N_φ, respectively. Then the number of basis functions for the z- and phi-current is equal to $NB_Z = N_Z\times(N_\varphi-1)$ and $NB_\varphi = (N_Z-1)\times N_\varphi$, respectively. In Fig. 3, the pair (N_Z, N_φ) varies from (2, 4) to (30, 60). Based on Fig. 3 we see that the results stabilize with an accuracy of about 1%.

Second, it is important to know how the resonant frequency behaves versus w_z. To study this, we segment the patch with $N_Z = 12$ and $N_\varphi = 24$ so that the full number of basis functions $NB = NB_Z + NB_\varphi = 540$. In Fig. 4 we present results for six different w_z values: $w_z = 20$ (red), 40 (magenta), 60 (orange), 80 (green), 160 (blue), and 320 μm (black).

Comparing these plots shows that, if $w_z/r_0 > 1.5$, then the HR frequency tends to a limiting value which corresponds to the 2-D case (see Table I). In view of this data, we have chosen $w_z = 160\ \mu$m in the systematic computations.

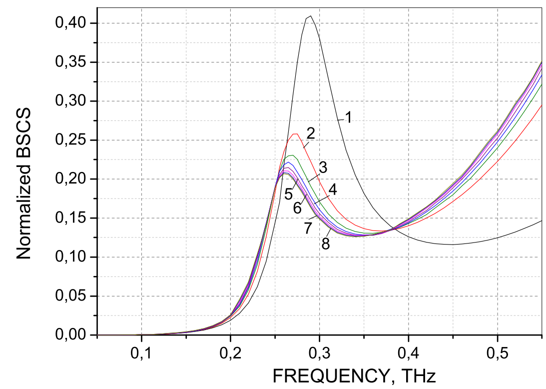

Fig. 3. Normalized $BSCS_{\varphi\varphi}$ versus frequency for different patch segmentations: N_Z and N_φ. and $\varepsilon_r = 2.4$, $r_0 = 50\ \mu$m, $\theta_s = 10°$, Wz = 160 μm, $W\varphi = 296.67\ \mu$m. 1—$N_z = 2$, $N_\varphi = 4$, 2—$N_z = 6$, $N_\varphi = 12$, 3—$N_z = 10$, $N_\varphi = 20$, 4—$N_z = 14$, $N_\varphi = 28$, 5—$N_z = 18$, $N_\varphi = 36$, 6—$N_z = 22$, $N_\varphi = 44$, 7—$N_z = 26$, $N_\varphi = 52$, 8—$N_z = 30$, $N_\varphi = 60$. $\gamma = 90°$.

TABLE I
Resonance Frequencies, THz

ε_r	Θ_s (deg.)	Graphene 3D	Graphene 2D	PEC 2D
1	10	0.329	0.327	0.432
1	40	0.432	0.449	0.602
2.4	10	0.271	0.258	0.332
2.4	40	0.351	0.352	0.449

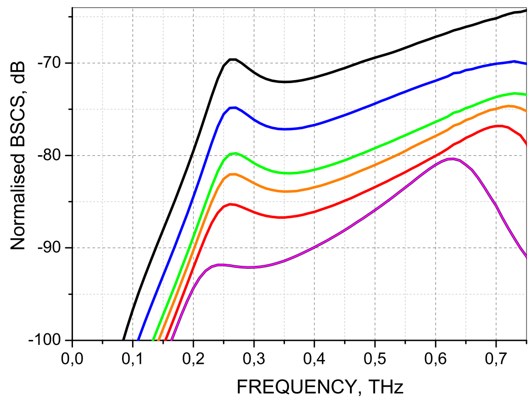

Fig. 4. Normalized $\text{BSCS}_{\varphi\varphi}$ versus frequency for different patch lengths: $w_z = 20$ (magenta), 40 (red), 60 (orange), 80 (green), 160 (blue), and 320 μm (black). $\varepsilon_r = 2.4$, $r_0 = 50$ μm, $\theta_s = 10°$, $\gamma = 90°$.

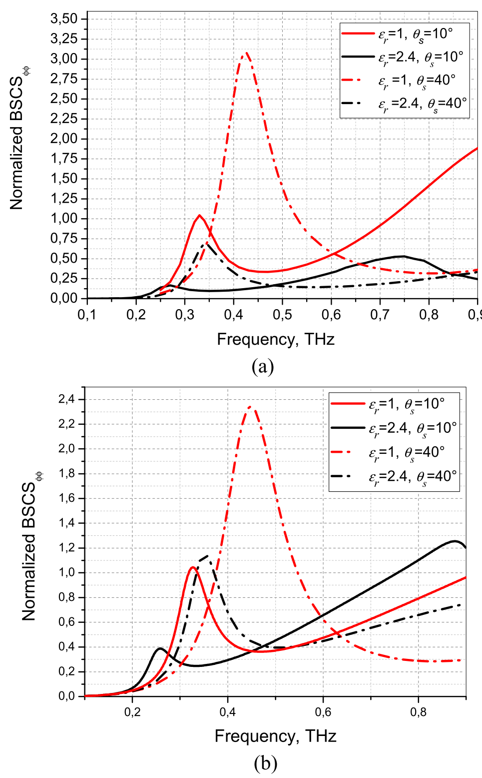

Fig. 5. Normalized $\text{BSCS}_{\varphi\varphi}$ versus frequency for (a) 3-D finite and (b) 2-D infinite graphene slotted cylinders on the surface of infinite dielectric rod.

Further in this section, the new 3-D model is validated against the 2-D model. The same set of geometrical and material parameters, namely, $\varepsilon_r = 1$ and $\varepsilon_r = 2.4$, $r_0 = 50$ μm, $\theta_s = 10°$ and $\theta_s = 40°$ is chosen, except for the length of the patch w_z, which is finite in the 3-D.

The $\text{BSCS}_{\varphi\varphi}$ in terms of frequency, both in the 3-D case (normalized by $2\pi^2 r_0 w_z$) and the 2-D case (normalized by πr_0) is presented in Fig. 5(a) and (b), respectively. The red curves correspond to $\varepsilon_r = 1$ and the black curves correspond to $\varepsilon_r = 2.4$. The dashed and dot-dashed curves correspond to $\theta_s = 10°$ and $\theta_s = 40°$, respectively.

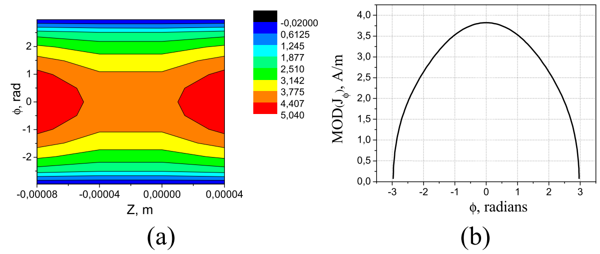

Fig. 6. ϕ-component of the resonant current distribution for $\varepsilon_r = 2.4$, $\theta_s = 10°$ for (a) 3-D model at $f = 0.271$ THz and (b) 2-D model at $f = 0.258$ THz.

All curves in Fig. 5(a) and (b) demonstrate a low-frequency resonance, corresponding to the HR on the Helmholtz mode, H_{00}. The resonance frequencies for the 2-D (infinite) and 3-D (finite) slotted graphene cylinders on dielectric rod and also for the infinite slotted PEC cylinder on a rod are collected in Table I. Note that the finite conductivity lowers the HR frequency, in agreement with (7).

A common feature is that the HR frequency decreases with the slot shrinking. In the LC-contour analogy [5], this means that the capacitance grows if the slot shrinks, which is logical. Similarly, the presence of dielectric rod also adds to the capacitance and lowers the HR frequency.

It is seen that there is a good agreement between the resonance frequencies for the 3-D and 2-D models. The discrepancy between finite and infinite graphene cylinder is in the range from 0.5% to 4.5%. Note that presented results correspond to the value $w_z/r_0 = 3.2$. This means that the finite graphene cylinder is quite long and that its inductance is close to the inductance of the infinite cylinder.

For smaller w_z/r_0 the effective inductance starts to vary and influences the HR frequency. It should also be mentioned that in the 3-D case there is a nonzero z-component of the electric current in the graphene cylinder. This component is zero in the 2-D case. It has been found that for H-polarized plane-wave incidence the influence of this z-component is negligible.

As for the different relative BSCS levels, there is the main factor that should be mentioned. Namely, in the 3-D case there are guided waves that are excited on the dielectric rod and take a part of power. In particular, two orthogonally polarized "principal" guided waves HE_{11} have no cutoff and can propagate at any frequency. In the 2-D configuration, the guided waves are not excited. It is also seen from Table I that the HR frequencies of both infinite and finite graphene slotted cylinders are shifted toward lower values in comparison with the 2-D PEC slotted cylinder [5], [6].

The ϕ-component of the resonant current for the 3-D and 2-D models is presented in Fig. 6(a) and (b), respectively. It is seen from Fig. 6(a) that the current amplitude pattern looks like a saddle due to the fact that this ϕ-current is singular at the edges $z = \pm w_z/2$ and goes to zero at the other two edges where $\phi = \pm\theta_s$

Fig. 6(b) demonstrates that in the 2-D case the current amplitude pattern is similar to the 3-D case (in the cross section, i.e., at $z = \text{const}$). The phase distribution (not shown

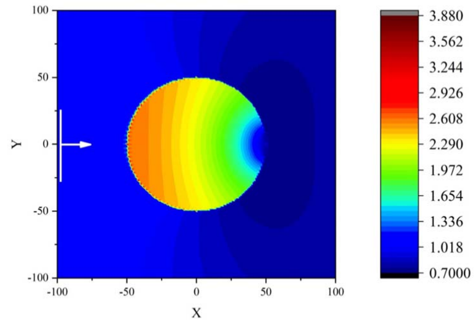

Fig. 7. Near-field pattern for magnetic component $|H_z|$ in the 2-D structure cross section for the case $\varepsilon_r = 2.4$, $\theta_s = 10^\circ$ for $f_{res} = 0.258$ THz.

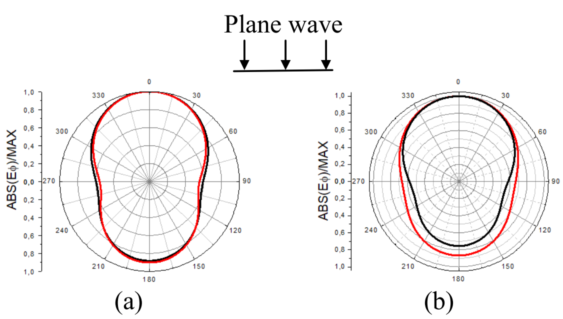

Fig. 8. Normalized far-field scattering patterns for the φ-component of the electric field in the xy plane in the case of (a) $\varepsilon_r = 1$, $\theta_s = 10^\circ$: black curve is for the 2-D case ($f_{\rm res} = 0.327$ THz) and red curve is for 3-D case ($f_{\rm res} = 0.329$ THz), and (b) $\varepsilon_r = 2.4$, $\theta_s = 10^\circ$: black curve is for the 2-D case ($f_{\rm res} = 0.258$ THz) and red curve is for 3-D case ($f_{\rm res} = 0.271$ THz).

here) tends to approach a constant with a deviation of about 0.15 radians in both the 3-D and the 2-D cases.

In Fig. 7, we present the HR magnetic near-field pattern. Note that the lines of $|H_z| =$ const coincide with the E-field force lines. These force lines are similar to the case of the slotted PEC cylinder (see [5], [6]). Nevertheless, the essential difference is that graphene becomes transparent in the THz wave range.

A comparison of far-field scattering patterns in the xy plane for the 2-D and 3-D cases is given in Fig. 8(a) and (b). The topologies involved are a graphene resonator without rod, i.e., $\varepsilon_r = 1$, $\theta_s = 10^\circ$, and with rod, i.e., $\varepsilon_r = 2.4$, $\theta_s = 10^\circ$. Black curves are for the 2-D case and red curves are for the 3-D case.

It is seen that the far-field patterns are in good agreement. The difference does not exceed 0.75 dB for the case $\varepsilon_r = 1$ and does not exceed 1.25 dB for the case $\varepsilon_r = 2.4$.

To demonstrate the 3-D far-field dependence versus the θ angle (see Fig. 1), in Fig. 9 we present the normalized far-field scattering pattern for the electric field φ-component in the xz plane in the case of $\varepsilon_r = 2.4$, $\theta_s = 10^\circ$ ($f_{res} = 0.271$ THz). It can be seen that the radiation pattern is close to omnidirectional one having a special behavior in the vicinity of axial directions, $\theta = 0^\circ$ and $\theta = 180^\circ$.

Here, one can be reminded that earlier it was shown in the numerical and analytical ways that in the far zone the E_θ component as a function of θ: 1) has local maxima

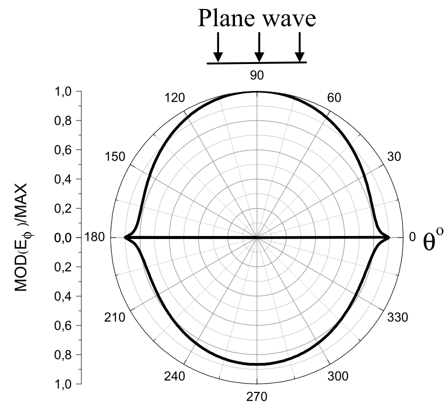

Fig. 9. Normalized far-field scattering pattern for the electric field φ-component in the xz plane in the 3-D case of $\varepsilon_r = 2.4$, $\theta_s = 10^\circ$ ($f_{res} = 0.271$ THz).

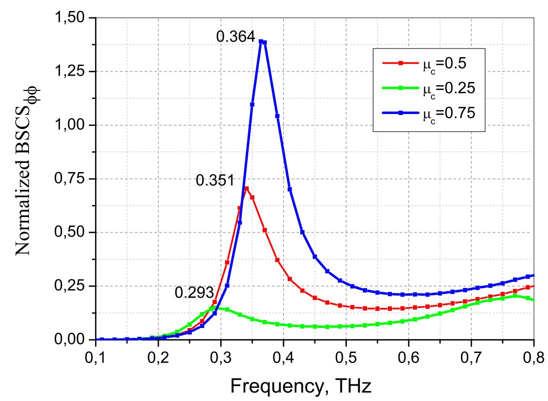

Fig. 10. Normalized BSCS$_{\varphi\varphi}$ versus the frequency for the 3-D finite graphene slotted cylinder on dielectric rod for different values of the graphene chemical potential: $\mu_c = 0.25$ (green), $\mu_c = 0.5$ (red), and $\mu_c = 0.75$ eV (blue). $\varepsilon_r = 2.4$, $\theta_s = 40^\circ$.

close to the axial direction and 2) goes to zero as $\ln^{-1}(\theta_s)$ and $\ln^{-1}(|\pi - \theta_s|)$, respectively. This happens due to the contribution of the $n = 1$ term of the Fourier series [34].

In order to demonstrate the tunability of the HR frequency in the case of graphene, in Fig. 10 the frequency dependence of the BSCS$_{\varphi\varphi}$ for several values of the chemical potential is shown.

The chemical potential scales linearly with the dc bias while the surface impedance of graphene is inversely proportional to this potential, see (5). It is seen that a smaller potential entails a smaller Q-factor for the HR.

V. Some Results for E-Polar Case

In Section IV, we have discussed the HR in the scattering of the H-polarized plane wave. Here, to excite both H- and E-polarizations at the same time we put $\gamma = 45^\circ$. The slotted graphene cylinder has parameters: $r_0 = 50$ μm, $\theta_s = 40^\circ$, $w_z = 160$ μm, W$\varphi = 244.35$ μm, $\varepsilon_r = 2.4$, and $\varepsilon_r = 1$. In Fig. 11, we present the BSCS$_{\varphi\varphi}$ (red and black solid lines) and BSCS$_{z\theta}$ (red and black dashed-dotted lines) for two ε_r values: $\varepsilon_r = 2.4$ (curves 1 and 3) and $\varepsilon_r = 1$ (curves 2 and 4). Note that the E-polar resonance is a half-wavelength resonance in the z-direction. As w_z is smaller than W$_\varphi$ the resonant

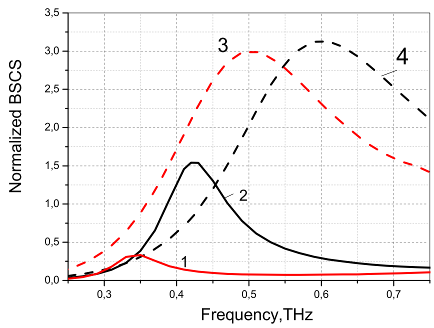

Fig. 11. Normalized BSCS$_{\varphi\varphi}$ (curves 1 and 2) and BSCS$_{z\theta}$ (curves 3 and 4) versus frequency. $r_0 = 50\ \mu$m, $\theta_s = 40°$, $W_z = 160\ \mu$m, $W_\varphi = 244.35\ \mu$m. $\varepsilon_r = 2.4$ (curves 1 and 3) and $\varepsilon_r = 1$ (curves 2 and 4), $\gamma = 45°$.

frequencies for the E-polar case are observed at higher frequencies in comparison with the H-polar case.

VI. Conclusion

A full-wave electromagnetic model for a novel tunable graphene resonator, promising in the sub-THz and low-THz region, has been presented. The HR is shaped as a finite-length slotted circular cylinder wrapped around a dielectric rod. This resonator displays a resonance on the slot mode H_{00} with a reasonably high Q-factor and an almost omnidirectional 3-D far-field scattering pattern. The important feature introduced by graphene is the tunability of the HR frequency. Such a resonator can be useful in the design of, for instance, sub-THz and low-THz sensors of small changes in the permittivity of either the host medium or the dielectric-rod material. This is because the HR frequency depends on both the mentioned values. Such a sensor can be seen as an alternative to existing sensors based on graphene strip arrays and plasmon-mode resonances [28].

Appendix A

A. Spectral GF for Electric Sheet Current

The components of the GF $\tilde{\mathbf{G}}^J(r_0, n, h)$ in the spectral domain take the following form:

$$\tilde{\mathbf{G}}^J(r_0, n, h) = \begin{bmatrix} \chi_{n\,zz}(r_0, \overline{h}) & \chi_{n\,z\phi}(r_0, \overline{h}) \\ \chi_{n\,\phi z}(r_0, \overline{h}) & \chi_{n\,\phi\phi}(r_0, \overline{h}) \end{bmatrix} \tag{18}$$

where

$$\chi_{n(zz)}(r_0, \overline{h}) = -\frac{\Delta_n^H(\overline{h})}{\Delta_n(\overline{h})}\frac{w_0}{k_0 r_0} \tag{19}$$

$$\chi_{n(z\phi)}(r_0, \overline{h}) = i\, w_0\, F_n \frac{\overline{\Delta}_n(\overline{h})}{\Delta_n(\overline{h})} + \frac{n\,\overline{h}\, w_0}{x_1^2}\frac{\Delta_n^H(\overline{h})}{\Delta_n(\overline{h})} \tag{20}$$

$$\chi_{n(z\phi)}(r_0, \overline{h}) = \chi_{n(\phi z)}(r_0, \overline{h}) \tag{21}$$

$$\begin{aligned}\chi_{n(\phi\phi)}(r_0, \overline{h}) = &-\frac{i\, w_0\, n\, \overline{h}\, k_0 r_0}{x_0\, x_1}\frac{\overline{\Delta}_n(\overline{h})}{\Delta_n(\overline{h})}\left[\frac{x_1}{x_0}F_n(\overline{h}) + \frac{x_0}{x_1}\Phi_n(\overline{h})\right] \\ &- \frac{(n\ \overline{h})^2 w_0\, k_0 r_0}{(x_0\, x_1)^2}\frac{\Delta_0^H(\overline{h})}{\Delta_n(\overline{h})} \\ &+ k_0 r_0\, w_0\, \Phi_n(\overline{h})\, F_n \frac{\Delta_n^E(\overline{h})}{\Delta_n(\overline{h})}\end{aligned} \tag{22}$$

$$\overline{\Delta}_n(\overline{h}) = n\,\overline{h}\left[x_1^{-2} - x_0^{-2}\right] \tag{23}$$

$$\Delta_n^E(\overline{h}) = -i\left[\Phi_n(\overline{h}) - \varepsilon_{r1} F_n(\overline{h})\right] \tag{24}$$

$$F_n(\overline{h}) = \frac{\gamma_1'(r_0)}{x_1\,\gamma_1(r_0)};\quad \Delta_n^H(\overline{h}) = i\left[\Phi_n(\overline{h}) - F_n(\overline{h})\right] \tag{25}$$

$$\Phi_n(\overline{h}) = \frac{\gamma_0'(r_0)}{x_0\,\gamma_0(r_0)};\quad \Delta_n(\overline{h}) = \overline{\Delta}_n(\overline{h}) - \Delta_n^E(\overline{h})\,\Delta_n^H(\overline{h}) \tag{26}$$

$$\gamma_{n0}(r, \overline{h}) = \frac{H_n^{(2)}(\tilde{k}_0 r)}{H_n^{(2)}(\tilde{k}_0 r_0)};\quad \gamma_{n1}(r, \overline{h}) = \frac{J_n(\tilde{k}_1 r)}{J_n(\tilde{k}_1 r_1)} \tag{27}$$

$$\widehat{k}_i^2 = k_0^2\{\varepsilon_{ri} - \overline{h}^2\};\quad x_i^2 = (k_0 r_0)^2\{\varepsilon_{ri} - \overline{h}^2\} \tag{28}$$

$$\overline{x}_1^2 = (k_0 r_1)^2\{\varepsilon_{r1} - \overline{h}^2\};\quad \overline{h} = h/k_0 \tag{29}$$

$$\varepsilon_{r\,i} = \begin{cases}\varepsilon_{r1} = \varepsilon_r, & r_1 < r < r_0 \\ \varepsilon_{r0} = 1, & r > r_0.\end{cases} \tag{30}$$

Here, $J_n(x)$ is a Bessel function and $H_n^{(2)}(x)$ is a Hankel function of the second kind, and ε_{ri} is the relative permittivity.

Appendix B

B. Resistive Term MoM Calculation

In the spatial domain the z- and ϕ-oriented PWS basis and test functions at (z_k^g, ϕ_k^g) lead to

$$\mathbf{J}_{i\,z}^g(z, \phi) = J_{i\,z}^g(z)\, J_{i\,z}^g(\phi)\, \mathbf{z}^0 \tag{31}$$

$$J_{i\,z}^g(z) = PWS(z, i, b, \mathbf{z}^0),\quad z_{i,1} \le z \le z_{i,2} \tag{32}$$

$$J_{i\,z}^g(\phi) = 1,\quad \overline{\varphi}_{i,1} \le \varphi \le \overline{\varphi}_{i,2} \tag{33}$$

$$\mathbf{J}_{k\,\varphi}^g(z, \phi) = J_{k\,\varphi}^g(z)\, J_{k\,\varphi}^g(\phi)\, \boldsymbol{\varphi}^0 \tag{34}$$

$$J_{k\,\varphi}^g(\varphi) = PWS(\varphi, k, g, \boldsymbol{\varphi}^0),\quad \overline{z}_{k,1} \le z \le \overline{z}_{k,2} \tag{35}$$

$$J_{k\,\varphi}^g(z) = 1,\quad \varphi_{k,1} \le \varphi \le \varphi_{k,2} \tag{36}$$

$$PWS(s, j, g, \mathbf{c}^0) = \frac{\sin[p_s(\Delta_s - \left|s - s_j^{gs}\right|)]}{\sin(p_s\Delta_s)}\mathbf{c}^0 \tag{37}$$

where

$$z_{i,1} \le z \le z_{i,2},\quad \overline{\varphi}_{i,1} \le \varphi \le \overline{\varphi}_{i,2} \tag{38}$$

$$\overline{z}_{i,1} \le z \le \overline{z}_{i,2},\quad \varphi_{i,1} \le \varphi \le \varphi_{i,2} \tag{39}$$

$$z_{i,2} = z_i^{bz} + \Delta z,\quad z_{i,1} = z_i^{bz} - \Delta z \tag{40}$$

$$\overline{\varphi}_{i,2} = \varphi_i^{bz} + \Delta\varphi/2,\quad \overline{\varphi}_{i,1} = \varphi_i^{bz} - \Delta\varphi/2 \tag{41}$$

$$\overline{z}_{i,2} = z_i^{bz} + \Delta z/2,\quad \overline{z}_{i,1} = z_i^{bz} - \Delta z/2 \tag{42}$$

$$\varphi_{i,1} = \varphi_i^{bz} - \Delta\varphi/2,\quad \varphi_{i,2} = \varphi_i^{bz} + \Delta\varphi/2 \tag{43}$$

$(z_i^{bz}, \varphi_i^{bz})$ and $(z_k^{b\varphi}, \varphi_k^{b\varphi})$ are the coordinates of the zth and φth basis functions, respectively. s stands for z or φ, $\mathbf{c}^0$ stands for $\mathbf{z}^0$ and ϕ^0, which are the unit vectors in the z- and ϕ-directions, $p_z = k_0 p_0$, $p_\varphi = k_0 r_0 p_z$, and $p_0 = \sqrt{(\varepsilon_r + 1)/2}$.

In these definitions, the elements of Z^R in (10) can be calculated in the spatial domain in explicit form as

$$Z_{i\,k}^{R,z,z} = Z^{Surf}\ \mathrm{I}_{\mathrm{i,\ k}}^{z}\ \ \mathrm{I}_{\mathrm{i,\ k}}^{z\varphi} \tag{44}$$

$$Z_{i\,k}^{R,\phi,\phi} = Z^{Surf}\ \mathrm{I}_{\mathrm{i,\ k}}^{\phi}\ \ \mathrm{I}_{\mathrm{i,\ k}}^{\varphi z} \tag{45}$$

where

$$\mathrm{I}_{\mathrm{i,\ k}}^{z} = \int_{z_{i,1}}^{z_{i,2}} J_{i,z}^t(z)\, J_{k,z}^b(z)\, dz \tag{46}$$

$$\mathrm{I}_{\mathrm{ik}}^{z\varphi} = \int_{\overline{\phi}_{i,1}}^{\overline{\phi}_{i,2}} J_{i,z}^{t}(\varphi)\ J_{k,z}^{b}(\varphi)d\varphi \tag{47}$$

$$\mathrm{I}_{\mathrm{ik}}^{\varphi} = \int_{\phi_{i,1}}^{\phi_{i,2}} J_{i,\varphi}^{t}(\varphi)\ J_{k,\varphi}^{b}(\varphi)d\varphi \tag{48}$$

$$\mathrm{I}_{\mathrm{i,\,k}}^{\varphi z} = \int_{\overline{Z}_{i,1}}^{\overline{Z}_{i,2}} J_{i,\phi}^{t}(z)\ J_{k,\phi}^{b}(z)\ dz. \tag{49}$$

Note that

$$Z_{i\,k}^{R,z,\phi} = Z_{i\,k}^{R,\phi,z} = 0. \tag{50}$$

Thanks to the fact that the z- and φ-basis functions are orthogonal, integrals (46)–(49) can be calculated in an explicit form as

$$\mathrm{I}_{\mathrm{i,\,i}}^{\mathrm{z}} = \frac{1}{2\,k_z\ \sin^2(k_z\Delta_z)}[2\,k_z\Delta_z - \sin(2k_z\Delta_z)] \tag{51}$$

$$\mathrm{I}_{\mathrm{i,\,i}}^{z\phi} = \Delta_\phi$$

$$\mathrm{I}_{\mathrm{i,\,i}-1}^{\mathrm{z}} = \frac{1}{2\ \sin^2(k_z\Delta_z)}\left[\frac{\sin(k_z\Delta_z)}{k_z} - \cos(k_z\Delta_z)\Delta_z\right] \tag{52}$$

$$\mathrm{I}_{\mathrm{i,\,i}+1}^{\mathrm{z}} = \mathrm{I}_{\mathrm{i,\,i}-1}^{\mathrm{z}};\quad \mathrm{I}_{\mathrm{i,\,i}-1}^{z\phi} = \mathrm{I1}_{\mathrm{i,\,i}+1}^{z\phi} = \Delta_\phi \tag{53}$$

$$\mathrm{I}_{\mathrm{i,\,i}}^{\varphi} = \frac{1}{2\,k_\varphi\ \sin^2(k_\varphi\Delta_\varphi)}\left[2\,k_\varphi\Delta_\varphi - \sin(2k_\varphi\Delta_\varphi)\right] \tag{54}$$

$$\mathrm{I}_{\mathrm{i,\,i}}^{\phi z} = \Delta_z \tag{55}$$

$$\mathrm{I}_{\mathrm{i,\,i}-1}^{\varphi} = \frac{1}{2\ \sin^2(k_\varphi\Delta_\varphi)}\left[\frac{\sin(k_\varphi\Delta_\varphi)}{k_\varphi} - \cos(k_\varphi\Delta_\varphi)\Delta_\varphi\right] \tag{56}$$

$$\mathrm{I}_{\mathrm{i,\,i}+1}^{\varphi} = \mathrm{I}_{\mathrm{i,\,i}-1}^{\varphi};\quad \mathrm{I}_{\mathrm{i,\,i}-1}^{\varphi z} = \mathrm{I1}_{\mathrm{i,\,i}+1}^{\varphi z} = \Delta_z. \tag{57}$$

The matrix elements for the other index combinations equal zero.

REFERENCES

[1] H. Helmholtz, *Theorie der Luftschwingungen in Rohren mit Offenen Enden*. Publ. Crelle, 1860.

[2] L. Rayleigh, "The theory of the Helmholtz resonator," *Proc. Roy. Soc. London A*, vol. 92, no. 638, pp. 265–275, 1916.

[3] H. Levine, "The wavelength of a spherical resonator with a circular aperture," *J. Acoust. Soc. Amer.*, vol. 23, no. 3, pp. 307–311, May 1951.

[4] P. J. B. Clarricoats, P. E. Green, and A. A. Oliner, "Slot-mode propagation in rectangular waveguide," *Electron. Lett.*, vol. 2, no. 8, pp. 307–308, Aug. 1966.

[5] E. I. Veliev, A. I. Nosich, and V. P. Shestopalov, "Propagation of electromagnetic waves in a cylindrical waveguide with a longitudinal slit," *Radio Eng. Electron. Phys.*, vol. 22, no. 3, pp. 29–35, 1977.

[6] A. I. Nosich and V. P. Shestopalov, "Waveguide properties of open metallized dielectric transmission lines of the cylindrical type," *Radio Eng. Electron. Phys.*, vol. 24, no. 10, pp. 1–9, 1979.

[7] A. I. Nosich, A. Y. Svezhentsev, and V. P. Shestopalov, "Electrodynamic analysis of the discrete spectrum of characteristic modes of a partially screened dielectric rod," *Sov. J. Communic. Technol. Electron.*, vol. 33, no. 3, pp. 18–26, 1988.

[8] A. I. Nosich and A. Y. Svezhentsev, "Physical features of wave propagation in cylindrical slot and strip lines," *Sov. J. Communic. Technol. Electron.*, vol. 35, no. 1, pp. 51–59, 1990.

[9] A. I. Nosich and A. Y. Svezhentsev, "Accurate computation of mode characteristics for open-layered circular cylindrical microstrip and slot lines," *Microw. Opt. Technol. Lett.*, vol. 4, no. 7, pp. 274–277, Jun. 1991.

[10] A. I. Nosich and V. P. Shestopalov, "Excitation of a partially shielded round dielectric rod by lumped sources," *Sov. Phys. Tech. Phys.*, vol. 28, no. 12, pp. 1421–1426, 1983.

[11] A. I. Nosich, Y. Okuno, and T. Shiraishi, "Scattering and absorption of E- and H-polarized plane waves by a circularly curved resistive strip," *Radio Sci.*, vol. 31, no. 6, pp. 1733–1742, Nov. 1996.

[12] S. S. Vinogradov, "Reflectivity of spherical shield," *Radiophys. Quantum Electron.*, vol. 26, no. 1, pp. 78–88, Jan. 1983.

[13] P. Chevalier, P. Bouchon, R. Haïdar, and F. Pardo, "Optical Helmholtz resonators," *Appl. Phys. Lett.*, vol. 105, no. 7, Aug. 2014, Art. no. 071110.

[14] P. Chevalier *et al.*, "Experimental demonstration of the optical Helmholtz resonance," *Appl. Phys. Lett.*, vol. 112, no. 17, Apr. 2018, Art. no. 171110.

[15] C. A. Valagiannopoulos, "Semi-analytic solution to a cylindrical microstrip with inhomogeneous substrate," *Electromagnetics*, vol. 27, no. 8, pp. 527–544, Nov. 2007.

[16] C. A. Valagiannopoulos, "Closed–form solution to the scattering of a skew strip field by metallic pin in a slab," *Prog. Electromagn. Res.*, vol. 79, pp. 1–21, 2008.

[17] P. A. Martin and A. Maurel, "Multiple scattering by random configurations of circular cylinders: Weak scattering without closure assumptions," *Wave Motion*, vol. 45, nos. 7–8, pp. 865–880, Sep. 2008.

[18] C. A. Valagiannopoulos, "Study of an electrically anisotropic cylinder excited magnetically by a straight strip line," *Prog. Electromagn. Res.*, vol. 73, pp. 297–325, 2007.

[19] X. B. Wu, "Scattering from an anisotropic cylindrical dielectric shell," *Int. J. Infr. Millim. Waves*, vol. 15, no. 10, pp. 1733–1744, Oct. 1994.

[20] D. L. Dault, N. V. Nair, J. Li, and B. Shanker, "The generalized method of moments for electromagnetic boundary integral equations," *IEEE Trans. Antennas Propag.*, vol. 62, no. 6, pp. 3174–3188, Jun. 2014.

[21] S. V. Dukhopelnykov, R. Sauleau, M. Garcia-Vigueras, and A. I. Nosich, "Combined plasmon-resonance and photonic-jet effect in the THz wave scattering by dielectric rod decorated with graphene strip," *J. Appl. Phys.*, vol. 126, no. 2, Jul. 2019, Art. no. 023104.

[22] S. V. Dukhopelnykov, R. Sauleau, and A. I. Nosich, "Integral equation analysis of terahertz backscattering from circular dielectric rod with partial graphene cover," *IEEE J. Quantum Electron.*, vol. 56, no. 6, pp. 1–8, Dec. 2020.

[23] A. Y. Svezhentsev and V. V. Kryzhanovskiy, "Patch shape influence upon radar cross section of a cylindrical microstrip antenna," *Prog. Electromagn. Res. B*, vol. 15, pp. 307–324, 2009.

[24] A. Y. Svezhentsev, V. V. Kryzhanovskiy, and G. A. E. Vandenbosch, "Cylindrical microstrip array antennas with slotted strip-framed patches," *Prog. Electromagn. Res.*, vol. 139, pp. 539–558, 2013.

[25] A. Y. Svezhentsev, P. J. Soh, S. Yan, and G. A. E. Vandenbosch, "Green's functions for probe-fed arbitrary-shaped cylindrical microstrip antennas," *IEEE Trans. Antennas Propag.*, vol. 63, no. 3, pp. 993–1003, Mar. 2015.

[26] A. Y. Svezhentsev, V. A. Kizka, and G. A. E. Vandenbosch, "Plane wave scattering by patches periodically placed on a dielectric rod surface," *Prog. Electromagn. Res. M*, vol. 82, pp. 61–71, 2019.

[27] A. Y. Svezhentsev, V. Volski, and G. A. E. Vandenbosch, "Plane wave scattering by cylindrically conformal periodic finite array with PEC and graphene patches," in *Proc. IEEE Ukrainian Microw. Week (UkrMW)*, Sep. 2020, pp. 692–695.

[28] D. Rodrigo *et al.*, "Mid-infrared plasmonic biosensing with graphene," *Science*, vol. 349, no. 6244, pp. 165–168, 2015.

[29] C. Dai *et al.*, "Hybridized radial and edge coupled 3D plasmon modes in self-assembled graphene nanocylinders," *Small*, vol. 27, Apr. 2021, Art. no. 2100079.

[30] G. W. Hanson, "Dyadic Green's functions and guided surface waves for a surface conductivity model of graphene," *J. Appl. Phys.*, vol. 103, no. 6, Mar. 2008, Art. no. 064302.

[31] A. I. Nosich, "Radiation conditions, limiting absorption principle, and general relations in open waveguide scattering," *J. Electromagn. Waves Appl.*, vol. 8, no. 3, pp. 329–353, 1994.

[32] M. Abramowitz and I. A. Stegun, *Handbook of Mathematical Functions*. New York, NY, USA: Dover, 1971.

[33] A. Y. Svezhentsev, "Excitation of a cylindrical microstrip antenna with two symmetrically located radiating elements," *Radiophys. Quantum Electron.*, vol. 48, no. 6, pp. 466–478, Jun. 2005.

[34] Y. Svezhentsev, "Some far field features of cylindrical microstrip antenna on an electrically small cylinder," *Prog. Electromagn. Res. B*, vol. 15, pp. 223–244, 2008.

Alexander Ye. Svezhentsev (Senior Member, IEEE) received the M.S. and Ph.D. degrees in radio physics from Kharkiv National University, Kharkiv, Ukraine, in 1979 and 1987, respectively, and the D.Sc. degree from the O. Y. Usikov Institute of Radiophysics and Electronics of the National Academy of Sciences of Ukraine (IRE NASU), Kharkiv, in 2011.

Since 1987, he has been with the Department of Diffraction Theory and Diffraction Electronics, IRE NASU, as a Junior Research Scientist, a Research Scientist, and a Senior Research Scientist, since 1992. From 2011 to 2013, he was a part-time Professor at Kharkiv National University of Radio Electronics (courses were in English). From 1998 to 2002, he was a Visiting Research Fellow at the Department of the Electrical Engineering, Katholieke Universiteit Leuven, Leuven, Belgium. His research interests include full-wave methods in electromagnetics, open metal-dielectric waveguides of complex cross section, groove guides and arrays, conformal array antennas with shaped patches, textile antennas, and micro- and nano-antennas.

Dr. Svezhentsev was a winner of the Ukrainian Young Scientist Award in 1991, the Young Scientist Award of the International Symposium on Antennas and Propagation (ISAP), Sapporo, Japan, in 1992, the Civilian Research and Development Foundation (CRDF) Travel Grant to attend the 22nd International Conference on IR&MM Waves, Wintergreen, VA, USA, in 1997, the G. Soros International Program Grant as a Research Group Leader in 1995, the IEEE Region 8 Travel Grant to visit the 5th European Workshop on Conformal Antennas, Bristol, U.K., and the FP7 Marie Curie Fellowship to carry on research on conformal antennas at the Katholieke Universiteit Leuven, from 2012 to 2014.

Sergii V. Dukhopelnykov (Member, IEEE) was born in Kharkiv, Ukraine, in 1982. He received the B.S., M.S., and Ph.D. degrees in mathematical modeling and numerical methods from Kharkiv National University, Kharkiv, in 2003, 2004, and 2010, respectively.

From 2007 to 2018, he was a Lecturer, a Senior Lecturer, and an Assistant Professor with the Department of Mathematics, National Technical University "Kharkiv Polytechnic Institute," Kharkiv. Since 2018, he has been a Senior Scientist with the Laboratory of Micro and Nano Optics, O. Y. Usikov Institute of Radiophysics and Electronics of the National Academy of Sciences of Ukraine (IRE NASU), Kharkiv, and a part-time Assistant Professor at the School of Mathematics, Kharkiv National University. His research interests are in singular integral equations, Nystrom methods, and patterned graphene scattering.

Dr. Dukhopelnykov was a recipient of the Ph.D. Award of the N. I. Akhiyezer Foundation, Kharkiv, in 2010, and the Young Scientist Prize of the International Conference on Mathematical Methods in Electromagnetic Theory, Kyiv, Ukraine, in 2018.

Vladimir Volski (Member, IEEE) received the M.S. and Ph.D. degrees from the Moscow Power Engineering Institute, Moscow, Russia, in 1987 and 1993, respectively.

In 1987, he joined the Antennas and Propagation of Radio Waves Division, Moscow Power Engineering Institute, as a Researcher. Since January 1996, he has been a Researcher at the ESAT-TELEMIC Division, Katholieke Universiteit Leuven, Leuven, Belgium. His main research interests include electromagnetic theory, computational electromagnetics, antenna design, and measuring of electromagnetic radiation.

Guy A. E. Vandenbosch (Fellow, IEEE) received the M.S. and Ph.D. degrees in electrical engineering from Katholieke Universiteit Leuven, Leuven, Belgium, in 1985 and 1991, respectively.

Since 1993, he has been a Lecturer and since 2005, a Full Professor at Katholieke Universiteit Leuven. From September to December 2014, he was a Visiting Professor at Tsinghua University, Beijing, China. His work has been published in ca. 360 papers in international journals and has led to ca. 410 papers at international conferences. His research interests are in the area of electromagnetic theory, computational electromagnetics, planar antennas and circuits, nano-electromagnetics, EM radiation, EMC, and bio-electromagnetics.

Dr. Vandenbosch has been a member of the "Management Committees" of the consecutive European Cooperation in Science and Technology (COST) actions on antennas since 1993. From 2017 to 2020, he was a member of the IEEE Electromagnetics Award Committee. Within the Antennas Center of Excellence (ACE) Network of Excellence of the European Union (EU) from 2004 to 2007, he was a member of the Executive Board and coordinated the activity on the creation of a European antenna software platform. After ACE, from 2007 to 2018, he chaired the EuRAAP Working Group on Software. From 1999 to 2004, he was the Vice-Chairman, from 2005 to 2009, he was the Secretary, and from 2010 to 2017, he was the Chairman of the IEEE Benelux Chapter on Antennas en Propagation. From 2002 to 2004, he was the Secretary of the IEEE Benelux Chapter on EMC. From 2012 to 2014, he was the Secretary of the Belgian National Committee for Radio-Electricity (URSI), where he is also in-charge of Commission E.

Alexander I. Nosich (Fellow, IEEE) was born in Kharkiv, Ukraine, in 1953. He received the M.S., Ph.D., and D.Sc. degrees in radio physics from Kharkiv National University, Kharkiv, in 1975, 1979, and 1990, respectively.

Since 1979, he has been with the O. Y. Usikov Institute of Radiophysics and Electronics of the National Academy of Sciences of Ukraine (IRE NASU), Kharkiv, where he is currently a Professor, a Principal Scientist, and the Head of the Laboratory of Micro and Nano Optics. Since 1992, he held many guest fellowships and professorships in the European Union (EU), U.K., Japan, Singapore, and Turkey. His research interests include the method of analytical regularization, propagation and scattering of waves, open waveguides, antennas and lasers, and the history of microwaves.

Prof. Nosich has been an initiator and the Technical Committee Chairman of the International Conference Series on Mathematical Methods in Electromagnetic Theory (MMET), Ukraine, since 1990. In 1995, he organized the IEEE AP-S East Ukraine Chapter, the first one in the former USSR. From 2006 to 2020, he represented Ukraine in the European Association on Antennas and Propagation. He was awarded the honorary title of Doctor Honoris Causa of the University of Rennes 1, France, in 2015, the Galileo Galilei Medal of the International Commission for Optics in 2017, and an elected Fellow of the Optical Society (OSA) in 2020. He was also a co-recipient of the 2017 National Prize of Ukraine in Science and Technology for the works "Photonics of Semiconductor and Dielectric Nanostructures" and the Solomon I. Pekar Award of NASU in the solid state physics theory in 2018.